

Predicting wheel forces using bearing capacity theory for general planar loads

J. P. Hambleton^{1,*} and S. A. Stanier²

¹ Department of Civil and Environmental Engineering, Northwestern University, Evanston, IL 60208, USA & ARC Centre of Excellence for Geotechnical Science and Engineering, The University of Newcastle, NSW 2308, Australia

² ARC Centre of Excellence for Geotechnical Science and Engineering, Centre for Offshore Foundation Systems, The University of Western Australia, Perth 6009, Australia

Abstract: This paper assesses the applicability of bearing capacity theory for evaluating the forces generated on wheels operating on clay under steady rolling conditions. Considering recent advances in bearing capacity theory, namely with respect to the interaction diagrams developed for general loading, a theoretical model for computing the horizontal force or torque from fundamental input parameters such as the vertical force (weight), wheel diameter, and undrained shear strength of the soil is presented. The predictions are compared with existing analytical solutions and data from laboratory testing, and reasonable agreement is demonstrated. The foremost conclusion is that bearing capacity theory can be used to obtain reasonable predictions of wheel forces analytically under any operating condition (driven, braked, or towed), provided the contact length and so-called contact angle, which defines the position of the contact interface, can be estimated. Aside from providing a rigorous and highly convenient framework for evaluating wheel forces under arbitrary loading, the analysis enables a natural physical interpretation of the mobility problem.

Keywords: soil-wheel interaction; mobility; bearing capacity; interaction diagrams; yield envelopes; clay

1. Introduction

Determining the forces on wheeled vehicles operating on soft terrain is a longstanding problem in off-road vehicle mobility for which empirical methods have historically prevailed over theoretical approaches. The most prevalent models rest on concepts attributed to Bekker (1956,

* Corresponding author. Address: Department of Civil and Environmental Engineering, McCormick School of Engineering and Applied Science, Northwestern University, 2145 Sheridan Road, Room A236, Evanston, IL 60208; Tel.: +1 847 491 4858; Email addresses: jphambleton@northwestern.edu (J. P. Hambleton), sam.stanier@uwa.edu.au (S. A. Stanier)

1960, 1969), who proposed that the basic parameters governing the response of terrain-vehicle systems can be assessed through specific tests using a set of devices known collectively as a bevameter. A large number of studies have refined and extended Bekker's semi-empirical models, many of which are summarised in the more recent works by Osetinsky and Shmulevich (2004), Shibly et al. (2005), Ding et al. (2014), and Gallina et al. (2016). Another large subset of empirical approaches is based on correlating vehicle performance directly to soil strength and deformability indices obtained from cone penetration tests (e.g., Freitag, 1965; Priddy, 1999; Maclaurin, 2007; Mason et al., 2016, Vahedifard et al. 2016). Rigorous models capable of relating wheel forces to fundamental soil mechanical properties are comparatively scarce but nevertheless can be found in the literature. These include the analytical and semi-analytical solutions proposed by Marshall (1968), Dagan and Tulin (1969), Collins (1972, 1978), Karafiath and Nowatzki (1978), Petryk (1983), Tordesillas and Shi (2000), and Hambleton and Drescher (2009a), as well as the numerical models developed using either finite element or discrete element methods by Yong et al. (1978), Liu and Wong (1996), Fervers (2004), Chiroux et al. (2005), Shoop et al. (2006a,b), Asaf et al. (2006), Hambleton and Drescher (2009a,b), Modenese (2013), Johnson et al. (2015), Xiao and Zhang (2016), Ozaki and Kondo (2016), and Nishiyama et al. (2016) among others. Alternative mathematical models, developed *ad hoc* from theoretical considerations or experimental evidence (e.g., Higa et al., 2015) or based on simplifying physical assumptions (e.g., Gray et al. 2016), can also be found in the literature.

With a view towards developing a rigorous and generalizable theory for predicting the forces for wheels operating on soft soils, this paper explores the postulate that the resultant forces acting on the soil-wheel interface can be assessed using bearing capacity theory for shallow foundations subjected to general planar loads, and that the wheel forces can in turn be evaluated through the applicable yield envelope. As will be demonstrated, this assumption leads to a theoretical formulation that can be easily implemented and involves only fundamental physical quantities. Moreover, the proposed model readily predicts the relationship between forces for any operating condition (driven, braked, or towed), without the need to consider the various cases separately. For simplicity, attention is restricted to quasi-static two-dimensional (plane strain) soil-wheel interaction and either rigid wheels or flexible wheels of a suitable nominal radius (cf. Fujimoto, 1977; Hambleton and Drescher, 2008). Focus is on soils exhibiting undrained behavior, such as saturated clay, whose strength can be characterised simply by the undrained shear strength s_u . Rough contact conditions are assumed, such that the shear stresses τ acting over the contact interface are limited by the undrained shear strength ($|\tau| \leq s_u$).

2. Proposed theoretical model

2.1. Foundation analogy

Figure 1 depicts the basic proposition of this paper, which is that the forces acting at the axis of a rolling wheel (Fig. 1a) can be assessed by considering an equivalent set of forces acting over the soil-wheel contact interface (Fig. 1b), which is deemed analogous to a shallow foundation subjected to general planar loads. The analogous shallow foundation has the same width as the soil-wheel contact interface, denoted by h , and its inclination is determined by the so-called contact angle ξ subtending the line bisecting the soil-wheel contact interface (see Fig. 1). The width and radius of the wheel, or nominal radius in the case of a flexible wheel, are denoted by b and r , respectively. The vertical force, horizontal force, and torque acting at the axis of the wheel are denoted by W , F , and Q , respectively, and they are considered positive when acting as shown in Fig. 1a. The normal force, tangential force, and moment acting over the analogous shallow foundation, positive in the sense shown in Fig. 1b, are denoted by V , H , and M , respectively.

The vast majority of mobility problems are concerned with the scenario in which relatively large, permanent deformations are induced in the soil, and thus the viability of the vehicle to operate comes into question. For this reason, it is reasonable, if not essential, to assume that contact forces V , H , and M combine in a way that they cause yielding in the soil, i.e., that the bearing capacity of the soil is reached. The combination of V , H , and M required to cause yielding is defined by the so-called yield envelope or VHM diagram.

2.2. Yield envelopes for shallow foundations

Evaluating the load combinations required to induce yielding has been the subject of various studies focused on the bearing capacity of shallow foundations, many of which are summarised in the works of Gottardi and Butterfield (1993), Taiebat and Carter (2000), and Shen et al. (2016). For undrained conditions and the case of a horizontal surface foundation resting on horizontal stratum of soil, Gourvenec (2007) proposed the following convenient expression for the yield envelope:

$$\frac{|H|}{H_{\max}} = \eta \sqrt{1 - \frac{M^2}{\mu^2 M_{\max}^2}} \quad (1)$$

where

$$\eta = \begin{cases} 1 & \text{for } 0 \leq \frac{V}{V_{\max}} \leq 0.5 \\ 1 - 4 \left(\frac{V}{V_{\max}} - \frac{1}{2} \right)^2 & \text{for } 0.5 \leq \frac{V}{V_{\max}} \leq 1 \end{cases} \quad (2)$$

$$\mu = 4 \left(\frac{V}{V_{\max}} - \frac{V^2}{V_{\max}^2} \right) \quad (3)$$

In Eqs. (1)-(3), the variables V_{\max} , H_{\max} , and M_{\max} are the so-called ultimate loads corresponding to single-component loading (e.g., $V = V_{\max}$ for $H = M = 0$). In this paper, the differences in capacity arising due to the inclination of the analogous foundation and the inclination of the soil surface relative to the analogous foundation (see Fig. 1) are neglected, and the ultimate loads are calculated as $V_{\max} = (2+\pi)s_{ub}bh$, $H_{\max} = s_{ub}bh$, and $M_{\max} = 0.7s_{ub}bh^2$ (Gourvenec, 2007). Based on the findings of Hambleton and Drescher (2012), who considered a similar foundation analogy for indentation, the effects of inclination are expected to be small.

The yield envelope defined by Eqs. (1)-(3) is plotted in Fig. 2. In the absence of a moment, the magnitude of the tangential force required to yield the soil remains constant over some range of the normal force and decreases as sharply as the normal force increases, eventually reaching $H = 0$ as the bearing capacity under purely normal loading, $V = V_{\max} = (2+\pi)s_{ub}bh$, is reached. For this special case, $M = 0$, the yield envelope is expressed simply as

$$\frac{|H|}{s_{ub}bh} = \begin{cases} 1 & \text{for } 0 \leq \frac{V}{(2+\pi)s_{ub}bh} \leq 0.5 \\ 1 - 4 \left[\frac{1}{(2+\pi)} \frac{V}{s_{ub}bh} - \frac{1}{2} \right]^2 & \text{for } 0.5 \leq \frac{V}{(2+\pi)s_{ub}bh} \leq 1 \end{cases} \quad (4)$$

2.3. Equilibrium and closure conditions

Three additional equations relating the contact forces V , H , and M to the wheel forces W , F , and Q are obtained considering static equilibrium:

$$W = V \cos \xi - H \sin \xi \quad (5)$$

$$F = V \sin \xi + H \cos \xi \quad (6)$$

$$Q = M + Wl \sin \xi - Fl \cos \xi \quad (7)$$

where l is the altitude given by

$$l = \sqrt{r^2 - \frac{h^2}{4}} \quad (8)$$

In total, the yield envelope of Eq. (1) combined with the equations of equilibrium, Eqs. (5)-(7) represent four equations that relate eight variables: the three wheel forces W , F , and Q ; the contact forces V , H , and M ; the contact length h ; and the contact angle ξ . Of the wheel forces, two out of three must be specified in order to prescribe a well-posed problem. For example, one may specify suitably normalised values for the vertical force and torque, W/s_{ubr} and Q/s_{ubr}^2 respectively, and then assess the corresponding horizontal force, H/s_{ubr} , that develops. A second case of practical interest would be to assess the torque required to achieve a particular horizontal force given a value for the vertical force. Hence, the problem involves a total of six unknowns, and one requires two additional equations or assumptions to arrive at a solution. These additional requirements, or closure conditions, are discussed further in Section 5, after considering existing analytical solutions (Section 3) and experimental data (Section 4).

3. Analysis of steady rolling by Collins (1972)

In this section, the notion of regarding soil-wheel interaction as an equivalent foundation problem involving general loading is assessed with respect to the analysis of a rolling rigid cylinder completed by Collins (1972). His investigation rested on the assumption of steady

motion and the construction on deformation mechanisms that approximate the arc of contact as a straight line, much like the foundation analogy depicted in Fig. 1. Based on the method of characteristics (slip lines), the mechanisms proposed by Collins (1972), reproduced for reference in Fig. 3, furnish approximate formulae relating the wheel forces W , F , and Q in parametric form. These formulae vary in complexity, in some cases requiring a numerical solution, and they are parameterised in terms of the angles α , β , and ε shown in Fig. 3, where generally $2(\alpha+\varepsilon)$ is the central angle defining the length of contact ($\varepsilon = 0$ in the mechanism of Fig. 3a).

3.1. Predicted wheel forces

The relationship between the wheel forces predicted by Collins' solutions is shown in Fig. 4. Clearly, the curves take rather peculiar forms that vary distinctly as the torque ranges from $Q < 0$ (braked wheel) to $Q > 0$ (driven wheel). For $Q < 0$ (braked wheel) and $Q = 0$ (towed wheel), Solution I is the only applicable solution. For $Q > 0$ (driven wheel), all three solutions are applicable, with Solution III being transitional between Solution I and Solution II. Irrespective of the value of the torque Q , the solutions are valid only over some range of forces, the extents of which are depicted qualitatively in Fig. 4. Outside these limits, the conditions governing the validity of the solution, such as the condition that region of rigid material attached to the wheel cannot be overstressed, prevent a solution from being constructed.

Perhaps the most peculiar aspect of the relationships plotted in Fig. 4 is that the functions are multi-valued. For example, with $W/s_{ubr} = 3$ and $Q/s_{ubr}^2 = 0.3$, four admissible values of the normalised horizontal force F/s_{ubr} , each corresponding to a different mode of deformation, are predicted. This curious behaviour can be attributed to the approximation of the arc of contact as a straight line, which in turn imposes specific constraints on the mechanisms used to deduce the forces. Indeed, Collins (1972) asserted that these solutions are applicable only to small contact angles, and for this reason he never plotted the solutions as shown in Fig. 4 but rather explored various linearised forms of the resulting equations.

3.2. Contact forces, contact length, and contact angle

For the present study, the value of Collins' solutions lies in the fact that the wheel forces, contact length $h = 2r\sin(\alpha+\varepsilon)$, and contact angle $\xi = \alpha$ are uniquely determined in each solution, and therefore the relationships between the equivalent contact forces V , H , and M can be

determined directly from the equations of equilibrium, Eqs. (5)-(7). The contact moment M is always zero in all cases by construction, a fact that is readily verified by computing M for each combination of wheel forces. It therefore suffices to plot the tangential contact force H against the normal contact force V , as shown in Fig. 5, which also plots the yield envelope given by Eq. (4). Plotted in this way, the curves corresponding to Collins' solutions take a form that is perhaps even more peculiar than that seen in Fig. 4. For example, in the case of the driven wheel ($Q > 0$), Solution III yields values that are identical to those obtained from Solution II. Overall, the solutions often fall well within the yield envelope from bearing capacity theory, or well outside of it.

In view of the curious nature of the curves shown in Fig. 5, which again can be attributed to the straight-line approximation for contact interface, attention is given to the emergent behaviour as the central angle $2(\alpha+\varepsilon)$, or 2α for Solution I, becomes small. Figures 6 and 7 show the full extent of valid solutions over a range of wheel torques, $-0.5 \leq Q/s_{ubr}^2 \leq 0.5$, considering limits on the central angle of $2(\alpha+\varepsilon) \leq 30^\circ$ and 10° , respectively. One can observe that as the central angle decreases, the solutions converge towards the yield envelope from bearing capacity theory. Furthermore, the range of applicability of Solution III becomes increasingly limited, although the necessity of the solution in attaining solutions close to the apex of the yield envelope, $H = 0$ and $V = V_{\max} = (2+\pi)s_u b h$, becomes apparent.

3.3. Implications

Based on the results shown in Figs. 5-7, one can conclude that Collins' solutions definitively support the analogy between rolling wheel and a shallow foundation subjected to general loading when the contact length is small compared to the radius. When the contact length is large, the analysis is inconclusive, as it is clear that the various mechanisms do not give reasonable solutions. In all cases, the contact moment is zero, an assumption that will prove useful in subsequent sections.

4. Laboratory tests by Freitag (1965)

The focus of this section is on the interpretation of the experimental data reported by Freitag (1965), who measured the forces on pneumatic tyres operating on clay and sand under various conditions. Freitag's comprehensive report tabulates the wheel forces W , F , and Q measured under steady rolling conditions for both a towed wheel ($Q = 0$) and a driven wheel, typically

with a controlled slip of $s = 20\%$ for clay. In Freitag's study, the slip s is defined as $s = 1 - v/\omega r_r$, where v is the linear wheel velocity, ω is the angular velocity, and r_r is the so-called rolling radius defined as the “forward advance per revolution of the loaded tire when towed on a plane, level, unyielding surface, divided by 2π ” ($r_r = r$ for a rigid wheel). A distinct feature of the study is that the undrained shear strength of the clay s_u was determined through triaxial testing. The measured strength, which ranged from $s_u = 11 \text{ kPa}$ to 36 kPa , correlated very well to the values of cone index in the instances where both sets of measurements were taken, and the latter were reported for each test.

4.1. Measured wheel forces

Figures 8 and 9 plot the wheel forces measured by Freitag (1965) using the dimensionless variables from the previous figures. Upon comparison of Figs. 8 and Fig. 4, one observes that the trends between the horizontal and vertical wheel forces are qualitatively similar to those predicted by Collins (1972) for the towed ($Q = 0$) and driven ($Q > 0$) conditions. Quantitatively, the experimental results differ significantly from the theoretical solutions. In particular, the maximum values of normalised vertical force W/s_{ubr} fall well outside the admissible range of the theoretical solutions. Such a discrepancy is not surprising considering that wheel flexibility and three-dimensional effects, both of which tend to increase the magnitude of the forces involved, are not considered in Collins' solutions. There are also likely to be significant viscous effects occurring in the clay on the interface in the rolling experiments due to the higher strain rates experienced in the tests compared to the triaxial tests used to characterise the undrained strength. Typically such viscous effects result in an increase in operative undrained strength of $\sim 5\text{-}20\%$ per logarithmic cycle of strain rate (e.g., Biscontin and Pestana, 2001). If the operative strength in Freitag's experiments was higher than measured in the corresponding triaxial tests due to strain rate effects, the normalised quantities in Fig. 8 would decrease, causing the measurements to tend closer to Collins' solutions.

4.2. Contact forces, contact length, and contact angle

Alone, the data reported by Freitag (1965) are insufficient to ascertain the relationship between the contact forces V , H , and M . In particular, no information regarding the contact length h or contact angle ξ is available for any of the tests. However, if one assumes $M = 0$ in consistence with the solutions by Collins (1972), the yield condition of Eq. (4) together with the three

equations of equilibrium, Eqs. (5)-(7), are sufficient to compute the four unknowns V , H , h , and ξ . With $M = 0$, Eq. (7) reduces to

$$Q = -Hl = -H\sqrt{r^2 - \frac{h^2}{4}} \approx -Hr \quad (9)$$

The approximation indicated in Eq. (9) is introduced not only to simplify the calculations but also in recognition of the fact that, for a flexible wheel, the contact length h , nominal wheel radius r , and altitude l may not be as strongly coupled as Eq. (8) would imply.

Figures 10-12 show the values of the normal contact force V , horizontal contact force H , contact length h , and contact angle ξ inferred from the test results. The contact forces plotted in Fig. 10 all lie precisely on the yield envelope as a result of having exactly as many equations as unknowns. For the towed wheel, the contact forces are given in all cases by $H = 0$ and $V = V_{\max} = (2+\pi)s_{ub}h$ as a direct consequence of Eq. (9), and thus the data are all gathered at the apex of the yield envelope. In contrast, the contact forces for the driven wheel are widely distributed across the envelope. As one might expect, the tests with the largest values of the normalised vertical force, marked by stars in Figs. 8-12, tend to produce values of the contact normal force that lie on the portion of the yield envelope over which the tangential contact force decreases. In other words, these points approach the capacity of the soil under purely normal loading. In Figs. 11 and 12, the inferred values of h and ξ are plotted against the corresponding values of wheel penetration, or so-called sinkage, measured by Freitag (1965), revealing fairly well-defined trends that degenerate as the penetration decreases.

4.3. Implications

While not entirely conclusive, the trends visible in Figs. 11 and 12 provide some level of validation of the theoretical framework proposed in this paper. Namely, one should expect that both the contact length and the contact angle should increase with increasing wheel penetration, and this expectation is fully met in Figs. 11 and 12. Likewise, the diminishing strength of the correlations for small wheel penetration is unsurprising given the well-known indeterminacy of the contact length for flexible wheels operating in soft soils (cf. Fujimoto, 1977; Hambleton and Drescher, 2008). On the other hand, while the trends are apparent, the inferred contact lengths are too large to be considered realistic. This overestimation of the contact length is

consistent with the discrepancy noted in comparing the experimental data to the solutions proposed by Collins (1972). While the influence of wheel flexibility is, to some extent, accounted for in the back-calculation of the contact length, three-dimensional effects are wholly neglected, and these effects may lead to an overestimation of the contact length through a commensurate underestimation of the forces involved. As observed earlier, the operating shear strength may also be underestimated, which would tend to result in an overestimation of the back-calculated contact lengths.

5. Model summary

5.1. Model implementation

The most straightforward means of implementing the proposed model is to specify the contact length h and contact angle ξ directly, and then to assess the wheel forces W , F , and Q from Eqs. (4)-(7), recognizing that Eq. (4) implicitly utilises the assumption that the contact moment M is zero. Results from the previous section suggest that both h and ξ relate strongly to the wheel penetration (sinkage), and this is well supported by findings from previous studies. In particular, the validity of this relationship for a towed wheel was demonstrated by Hambleton and Drescher (2008, 2009a, 2012), who also reflected on the pathological nature of the two-dimensional problem as compared to the three-dimensional problem (2009b). For steady motion of a towed, rigid wheel, the contact length is approximated as the chord length spanning the lowermost part of the wheel and the point of intersection with undisturbed soil surface, as shown in Fig. 13 (cf. Hambleton and Drescher, 2009a):

$$h = \sqrt{2\delta r} \quad (10)$$

The corresponding contact angle is given by

$$\xi = \sin^{-1} \left(\sqrt{\frac{\delta}{2r}} \right) \quad (11)$$

Equation (11) is plotted together with the data of Freitag (1965) in Fig. 12, which shows that Eq. (11) generates contact angles reasonably close to the experimental results. The apparent deviations, especially at low values of wheel penetration, are to be expected considering the flexibility of the tyre used in the tests.

Predictions of the wheel forces obtained with the proposed model, given by combining Eqs. (4)-(6) and Eqs. (8)-(11), are plotted in Fig. 14. Overall, the curves are similar to those shown in Fig. 4 for the solutions proposed by Collins (1972). The curves from the proposed model exhibit smaller curvature and, most notably, a single-valued nature for all possible values of the wheel torque. In Fig. 14, the curves are bounded on the lower left by the physical condition that the horizontal contact force H cannot exceed the maximum $H_{\max} = s_{ubh}$, and they are bounded on the upper right by an arbitrarily selected restriction on the wheel penetration (sinkage) of $\delta \leq r/4$, imposed in recognition of the model's limitations as the penetration becomes large. It should be emphasised that all of the predictions, parameterised in terms of the normalised wheel penetration δ/r , are plotted based on the same set of equations, and thus the model provides a single comprehensive framework for addressing each of the various cases (driven, braked, and towed).

5.2. Physical interpretation

As depicted in Fig. 15, the proposed model also provides a natural physical interpretation of the mobility problem. The assumption that the contact moment M is zero requires that the line of action of resultant contact force passes through the centre of the equivalent foundation, and this line of action passes either behind the centre of the wheel when braked (Fig. 14a) or in front of the wheel's centre when driven (Fig. 14b). For a towed wheel, the line of action passes directly through the wheel's centre. In each case, the magnitude of the contact forces is dictated directly by the yield envelope.

6. Conclusions

The basic proposition of this paper is that the forces developing on a rolling wheel operating on soft soil can be assessed by considering an equivalent shallow foundation subjected to general planar loading. Combined with suitable estimates for the two primary geometric variables appearing in the model, the contact length h and contact angle ξ , this analogy leads to a comprehensive yet simple theoretical framework for predicting wheel forces in any

operating condition (driven, braked, and towed). Namely, Eqs. (4)-(6) and (8)-(11) constitute a complete theoretical model for predicting the wheel forces W , F , and Q from three fundamental inputs: the undrained shear strength of the soil s_u , the wheel width b , and the wheel radius r . The model is parametrized in terms of the wheel penetration (sinkage) δ , which is not required as an input but nevertheless imposes limits on the range of validity of the solution, as illustrated in Fig. 14.

While the proposed model remains to be fully validated by laboratory and field tests in which the length and position of the contact interface are somehow determined, initial comparisons with existing analytical solutions and experimental data provide a partial validation. Attention in this study was directed at the two-dimensional (plane strain) problem and fine-grained soils exhibiting undrained behaviour, but the potential to extend the model to other materials (e.g., sand) is evident. Indeed, a key aspect of the proposed model is that it takes direct advantage of the relatively mature body of knowledge pertaining to the bearing capacity of shallow foundations. Existing works on the bearing capacity of three-dimensional problems (e.g., Gourvenec, 2007) may prove very useful in refining the model to obtain quantitative as well as qualitative agreement with laboratory data for narrow wheels, such as that reported by Freitag (1965).

A key assumption utilised repeatedly in this study, and implemented implicitly in the solutions proposed by Collins (1972), is that the contact moment is zero. This simplifies the computations considerably, but an open question remains as to whether this assumption is correct. The proposed model can easily account for the effect of a non-zero moment, provided it can be estimated.

Acknowledgements

The authors gratefully acknowledge the financial support provided by the Australian Research Council (ARC) through the ARC Centre of Excellence for Geotechnical Science and Engineering (CE110001009). The first author also acknowledges support from an ARC Discovery Early Career Research Award (DE160100328).

References

- Asaf, Z., Shmulevich, I., and Rubinstein, D. (2006). Predicting soil-rigid wheel performance using distinct element methods. *Transactions of the ASABE*, 49(3), 607-616.

- Bekker, M.G. (1956). *Theory of Land Locomotion*, University of Michigan Press, Ann Arbor.
- Bekker, M.G. (1960). *Off-the-Road Locomotion*, University of Michigan Press, Ann Arbor.
- Bekker, M.G. (1969). *Introduction to Terrain-Vehicle Systems*, University of Michigan Press, Ann Arbor.
- Biscontin, G., and Pestana, J.M. (2001). Influence of peripheral velocity on vane shear strength of an artificial clay. *Geotechnical Testing Journal*, 24(4), 3423-429.
- Chiroux, R.C., Foster, W.A., Johnson, C.E., Shoop, S.A., and Raper, R.L. (2005). Three-dimensional finite element analysis of soil interaction with a rigid wheel. *Applied Mathematics and Computation*, 162(2), 707-722.
- Collins, I.F. (1972). A simplified analysis of the rolling of a cylinder on a rigid/perfectly plastic half-space. *International Journal of Mechanical Sciences*, 14(1), 1-14.
- Collins, I.F. (1978). On the rolling of a rigid cylinder on a rigid/perfectly plastic half-space. *Journal de Mécanique appliquée*, 2(4), 431-448.
- Dagan, G., and Tulin, M.P. (1969). A study of the steady flow of a rigid-plastic clay beneath a driven wheel. *Journal of Terramechanics*, 6(2), 9-27.
- Ding, L., Gao, H., Deng, Z., Li, Y., and Liu, G. (2014). New perspective on characterizing pressure-sinkage relationship of terrains for estimating interaction mechanics. *Journal of Terramechanics*, 52, 57-76.
- Fervers, C.W. (2004). Improved FEM simulation model for tire-soil interaction. *Journal of Terramechanics*, 41(2-3), 87-100.
- Freitag, D.R. (1965). *A Dimensional Analysis of the Performance of Pneumatic Tires on Soft Soils*, Technical Report No. 3-688, US Army Engineer Waterways Experiment Station, Vicksburg.
- Fujimoto, Y. (1977). Performance of elastic wheels on yielding cohesive soils. *Journal of Terramechanics*, 14(4), 191-210.
- Gallina, A., Krenn, R., and Schäfer, B. (2016). On the treatment of soft soil parameter uncertainties in planetary rover mobility simulations. *Journal of Terramechanics*, 63, 33-47.
- Gottardi, G., and Butterfield, R. (1993). On the bearing capacity of surface footings on sand under general planar loads. *Soils and Foundations*, 33(3), 68-79.
- Gourvenec, S. (2007). Shape effects on the capacity of rectangular footings under general loading. *Géotechnique*, 57(8), 637-646.
- Gray, J.P., Vantsevich, V. V., and Paldan, J. (2016). Agile tire slippage dynamics for radical enhancement of vehicle mobility. *Journal of Terramechanics*, 65, 14-37.

- Hambleton, J.P. and Drescher, A. (2008). *Development of Improved Test Rolling Methods for Roadway Embankment Construction—Final Report*, Minnesota Department of Transportation, Research Services Section, St. Paul.
- Hambleton, J.P., and Drescher, A. (2009a). Modeling wheel-induced rutting in soils: Rolling. *Journal of Terramechanics*, 46(2), 34-47.
- Hambleton, J.P., and Drescher, A. (2009b). On modeling a rolling wheel in the presence of plastic deformation as a three- or two-dimensional process. *International Journal of Mechanical Sciences*, 51(11-12), 846-855.
- Hambleton, J.P., and Drescher, A. (2012). Approximate model for blunt objects indenting cohesive-frictional material. *International Journal for Numerical and Analytical Methods in Geomechanics*, 36(3), 249-271.
- Higa, S., Nagaoka, K., Nagatani, K., and Yoshida, K. (2015). Measurement and modeling for two-dimensional normal stress distribution of wheel on loose soil. *Journal of Terramechanics*, 62, 63-73.
- Johnson, J.B., Kulchitsky, A.V., Duvoy, P., Iagnemma, K., Senatore, C., Arvidson, R.E., and Moore, J. (2015). Discrete element method simulations of Mars Exploration Rover wheel performance. *Journal of Terramechanics*, 62, 31-40.
- Liu, C.H., and Wong, J.Y. (1996). Numerical simulations of tire-soil interaction based on critical state soil mechanics. *Journal of Terramechanics*, 33(5), 209-221.
- Karafiath, L.L., Nowatzki, E.A. (1978). *Soil Mechanics for Off-road Vehicle Engineering*, Trans Tech Publications, Clausthal.
- MacLaurin, B. (2007). Comparing the NRMM (VCI), MMP and VLCI traction models. *Journal of Terramechanics*, 44, 43-51.
- Marshall, E.A. (1968). Rolling contact with plastic deformation. *Journal of the Mechanics and Physics of Solids*, 16(4), 243-254.
- Mason, G.L., Vahedifard, F., Robinson, J.D., Howard, I.L., McKinley, G.B., and Priddy, J.D. (2016). Improved sinkage algorithms for powered and unpowered wheeled vehicles operating on sand. *Journal of Terramechanics*, 67, 25-36.
- Modenese, C. (2013). *Numerical Study of the Mechanical Properties of Lunar Soil by the Discrete Element Method*. PhD Thesis. University of Oxford, Oxford.
- Nishiyama, K., Nakashima, H., Yoshida, T., Ono, T., Shimizu, H., Miyasaka, J., and Ohdoi, K. (2016). 2D FE-DEM analysis of tractive performance of an elastic wheel for planetary rovers, *Journal of Terramechanics*, 64, 23-35.

- Osetinsky, A., and Shmulevich, I. (2004). Traction performance simulation of a pushed/pulled driven wheel. *Transactions of the ASAE*, 47(4), 981-994.
- Ozaki, S., and Kondo, W. (2016). Finite element analysis of tire traveling performance using anisotropic frictional interaction model. *Journal of Terramechanics*, 64, 1-9.
- Petryk, H. (1983). Slip-line field analysis of the rolling contact problem at high loads. *International Journal of Mechanical Sciences*, 25(4), 265-275.
- Priddy, J.D. (1999). *Improving the Traction Prediction Capabilities in the NATO Reference Mobility Model (NRMM)*, Technical Report No. GL-99-8, US Army Engineer Waterways Experiment Station, Vicksburg.
- Shen, Z., Feng, X., and Gourvenec, S. (2016). Undrained capacity of surface foundations with zero-tension interface under planar V-H-M loading. *Computers and Geotechnics*, 73, 47-57.
- Shibly, H., Iagnemma, K., and Dubowsky, S. (2005). An equivalent soil mechanics formulation for rigid wheels in deformable terrain, with application to planetary exploration rovers. *Journal of Terramechanics*, 42(1), 1-13.
- Shoop, S.A., Richmond, P.W., and Lacombe, J. (2006a). Overview of cold regions mobility modeling at CRREL. *Journal of Terramechanics*, 43(1), 1-26.
- Shoop, S.A., Haehnel, R., Janoo, V., Harjes, D., and Liston, R. (2006b). Seasonal deterioration of unsurfaced roads. *Journal of Geotechnical and Geoenvironmental Engineering*, 132(7), 852-860.
- Taiebat, H.A., and Carter, J.P. (2000). Numerical studies of the bearing capacity of shallow foundations on cohesive soil subjected to combined loading. *Géotechnique*, 50(4), 409-418.
- Tordesillas, A., and Shi, J. (2000). Frictionless rolling contact of a rigid circular cylinder on a semi-infinite granular material. *Journal of Engineering Mathematics*, 37(1-3), 231-252.
- Vahedifard, F., Robinson, J.D., Mason, G.L., Howard, I.L., and Priddy, J.D. (2016). Mobility algorithm evaluation using a consolidated database developed for wheeled vehicles operating on dry sands. *Journal of Terramechanics*, 63, 13-22.
- Xiao, W., and Zhang, Y. (2016). Design of manned lunar rover wheels and improvement in soil mechanics formulas for elastic wheels in consideration of deformation. *Journal of Terramechanics*, 65, 61-71.
- Yong, R.N., Fattah, E.A., and Boonsinsuk, P. (1978). Analysis and prediction of tyre-soil interaction and performance using finite elements. *Journal of Terramechanics*, 15(1), 43-63.

Figure Captions

Figure 1. Schematic showing (a) wheel forces and (b) forces on the analogous shallow foundation.

Figure 2. Yield envelope showing the tangential force as a function of the normal force for selected values of the moment.

Figure 3. Solutions proposed by Collins (1972) to relate wheel forces for steady rolling of a rigid cylinder.

Figure 4. Relationship between horizontal wheel force and vertical wheel force for a braked ($Q < 0$), towed ($Q = 0$), and driven ($Q > 0$) wheel as predicted by solutions proposed by Collins (1972).

Figure 5. Relationship between the tangential contact force and normal contact force for solutions proposed by Collins (1972).

Figure 6. Valid combinations of contact forces from solutions proposed by Collins (1972) for central angle $2(\alpha + \varepsilon) \leq 30^\circ$.

Figure 7. Valid combinations of contact forces from solutions proposed by Collins (1972) for central angle $2(\alpha + \varepsilon) \leq 10^\circ$.

Figure 8. Horizontal wheel force versus vertical wheel force based on test results reported by Freitag (1965) for a 9.00-14 tire.

Figure 9. Torque force versus vertical wheel force based on test results reported by Freitag (1965) for a 9.00-14 tire.

Figure 10. Contact forces inferred from the test results reported by Freitag (1965).

Figure 11. Contact lengths inferred from the test results reported by Freitag (1965) and plotted as a function of wheel penetration (sinkage).

Figure 12. Contact angles inferred from the test results reported by Freitag (1965) and plotted as a function of wheel penetration (sinkage).

Figure 13. Approximation of contact length h and contact angle ξ as functions of wheel penetration δ (cf. Hambleton and Drescher, 2009a).

Figure 14. Relationship between horizontal force and vertical force for a braked ($Q < 0$), towed ($Q = 0$), and driven ($Q > 0$) wheel as predicted by the proposed model.

Figure 15. Physical interpretation of the proposed model: (a) braked wheel ($Q < 0$); and (b) driven wheel ($Q > 0$).

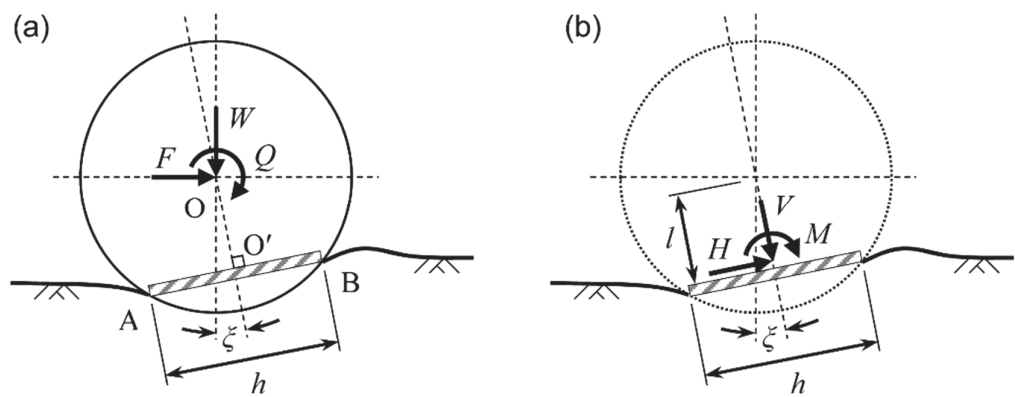


Figure 1. Schematic showing (a) wheel forces and (b) forces on the analogous shallow foundation.

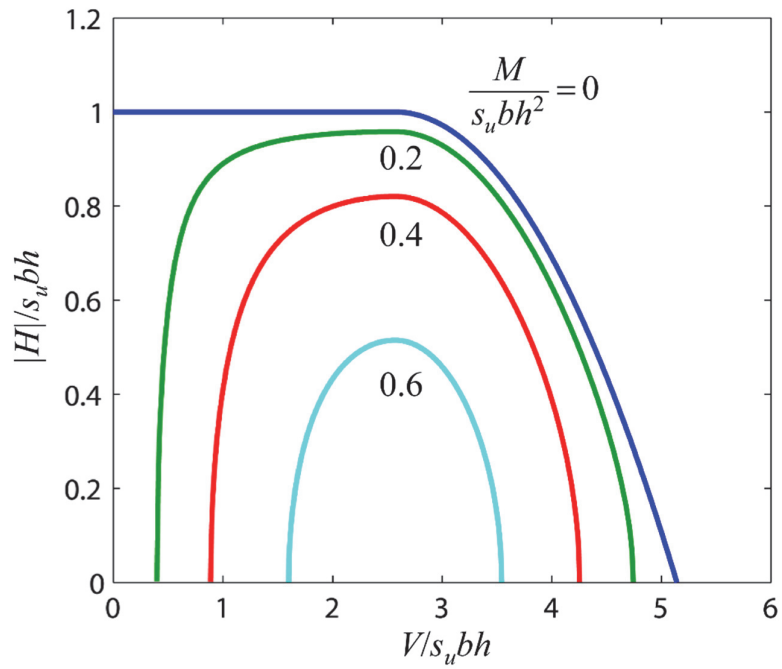


Figure 2. Yield envelope showing the tangential force as a function of the normal force for selected values of the moment.

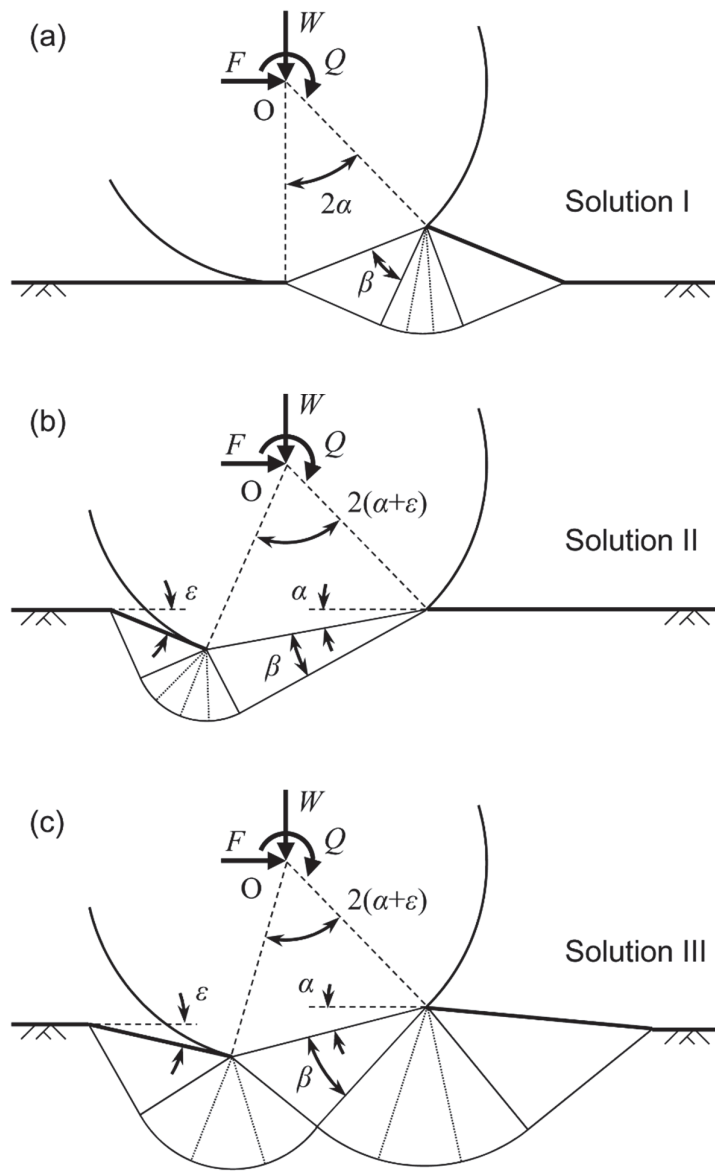


Figure 3. Solutions proposed by Collins (1972) to relate wheel forces for steady rolling of a rigid cylinder.

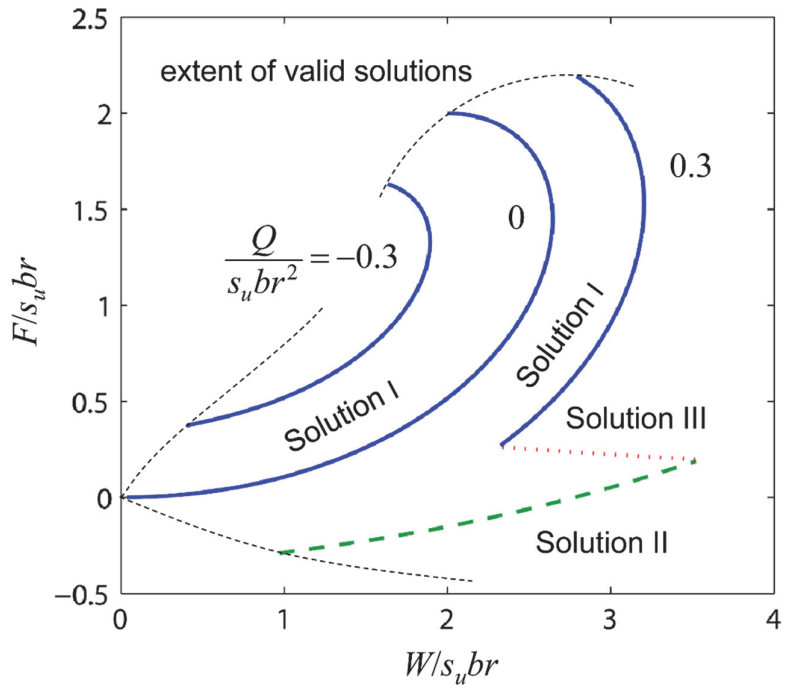


Figure 4. Relationship between horizontal wheel force and vertical wheel force for a braked ($Q < 0$), towed ($Q = 0$), and driven ($Q > 0$) wheel as predicted by solutions proposed by Collins (1972).

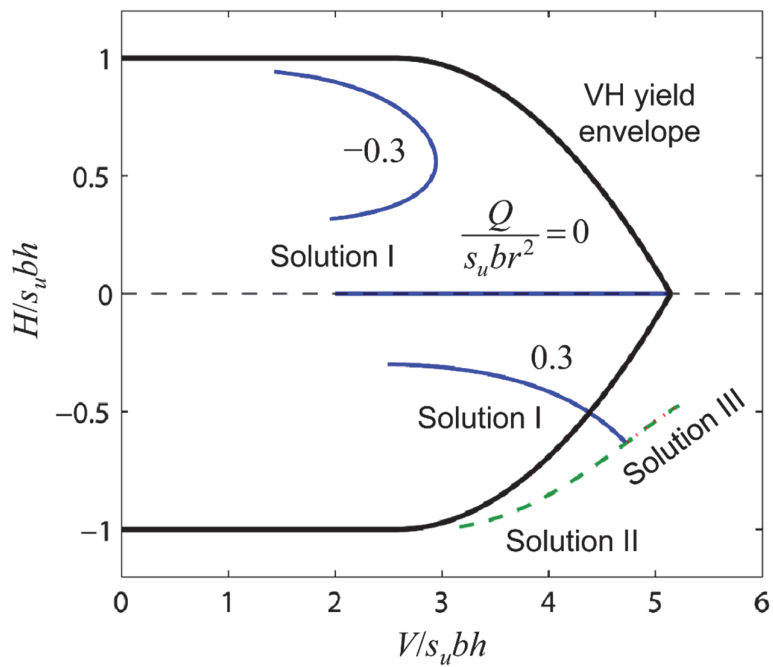


Figure 5. Relationship between the tangential contact force and normal contact force for solutions proposed by Collins (1972).

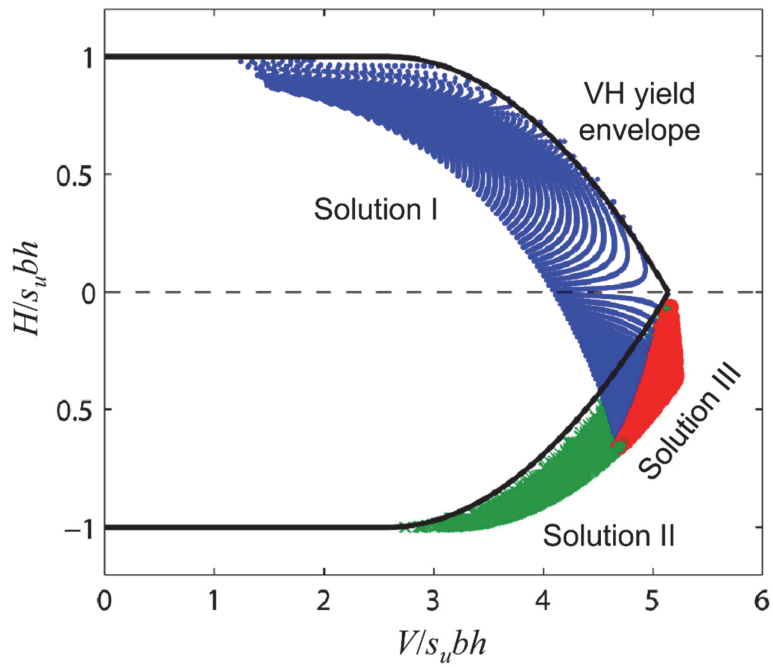


Figure 6. Valid combinations of contact forces from solutions proposed by Collins (1972) for central angle $2(\alpha+\varepsilon) \leq 30^\circ$.

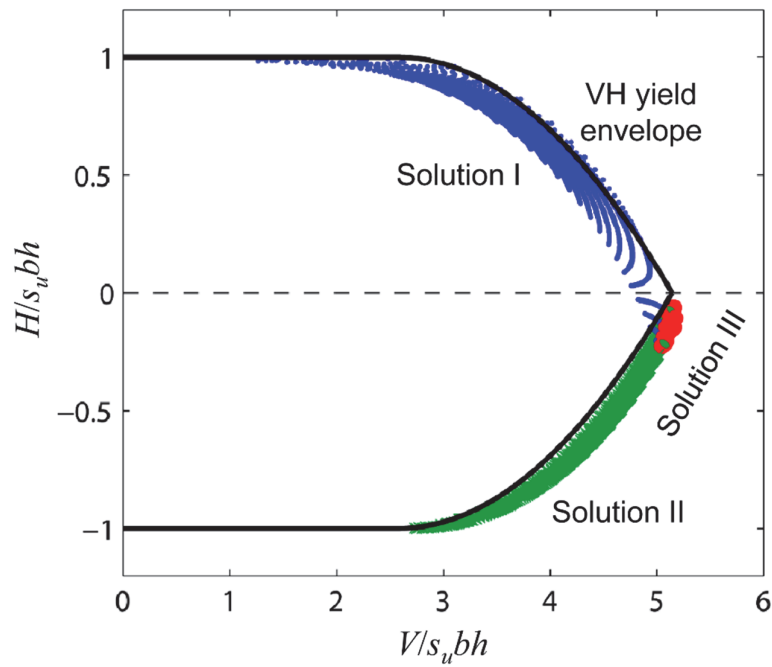


Figure 7. Valid combinations of contact forces from solutions proposed by Collins (1972) for central angle $2(\alpha+\varepsilon) \leq 10^\circ$.

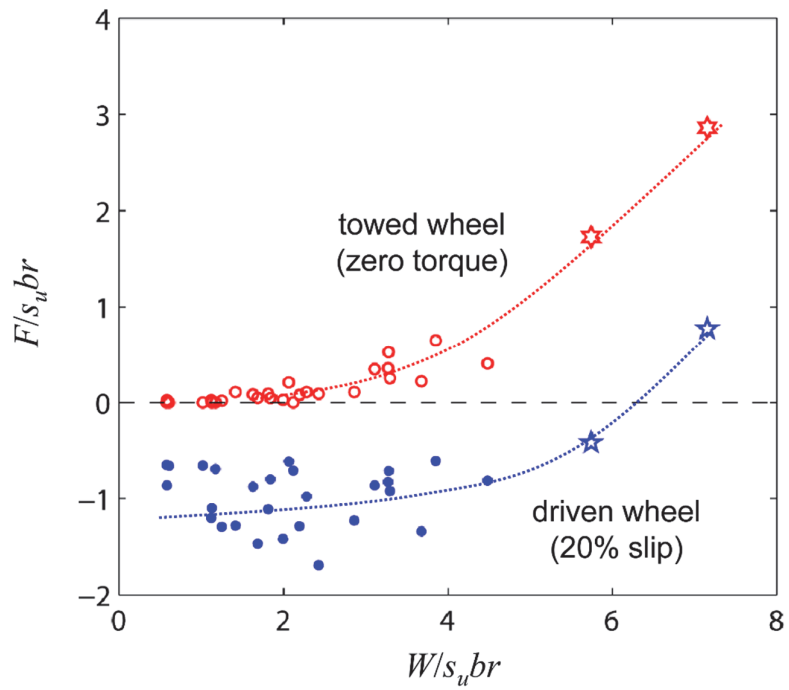


Figure 8. Horizontal wheel force versus vertical wheel force based on test results reported by Freitag (1965) for a 9.00-14 tire.

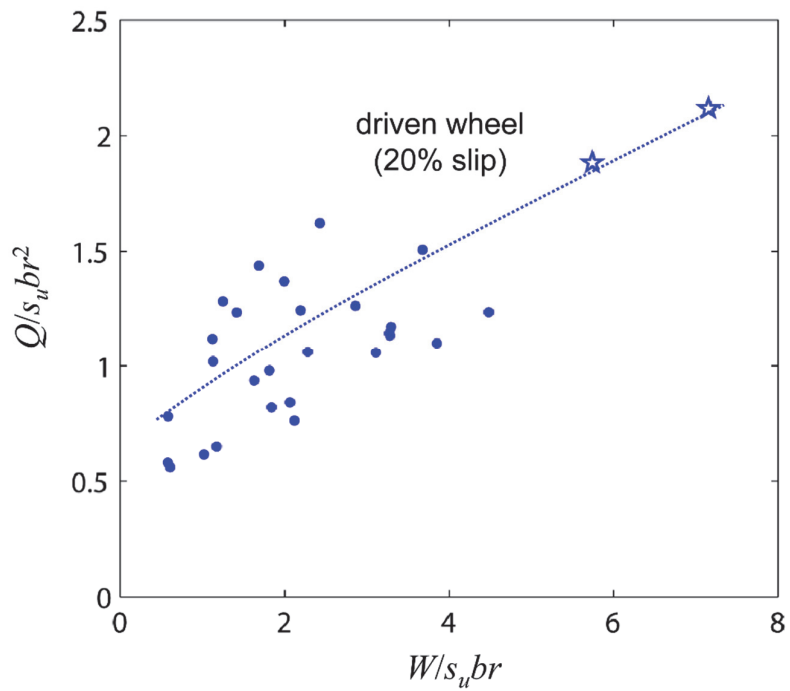


Figure 9. Torque force versus vertical wheel force based on test results reported by Freitag (1965) for a 9.00-14 tire.

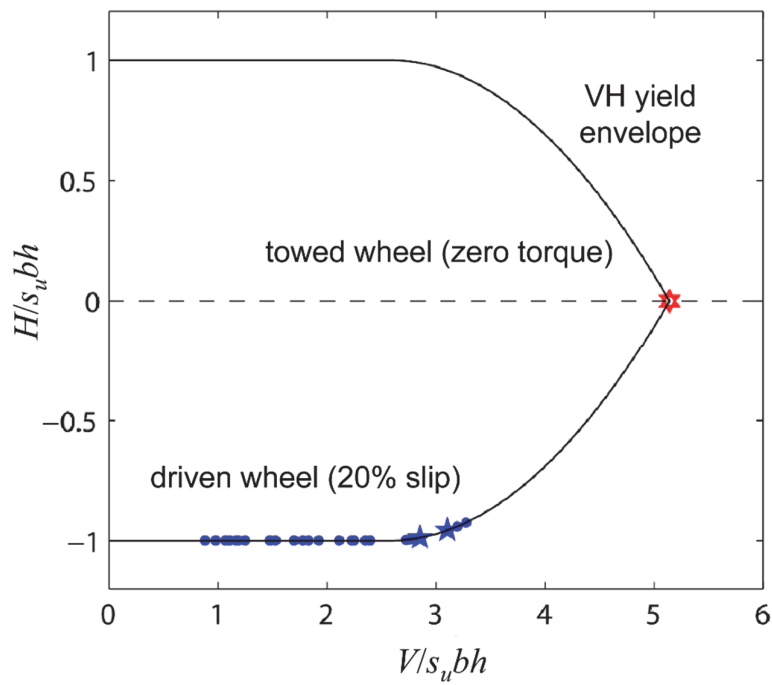


Figure 10. Contact forces inferred from the test results reported by Freitag (1965).

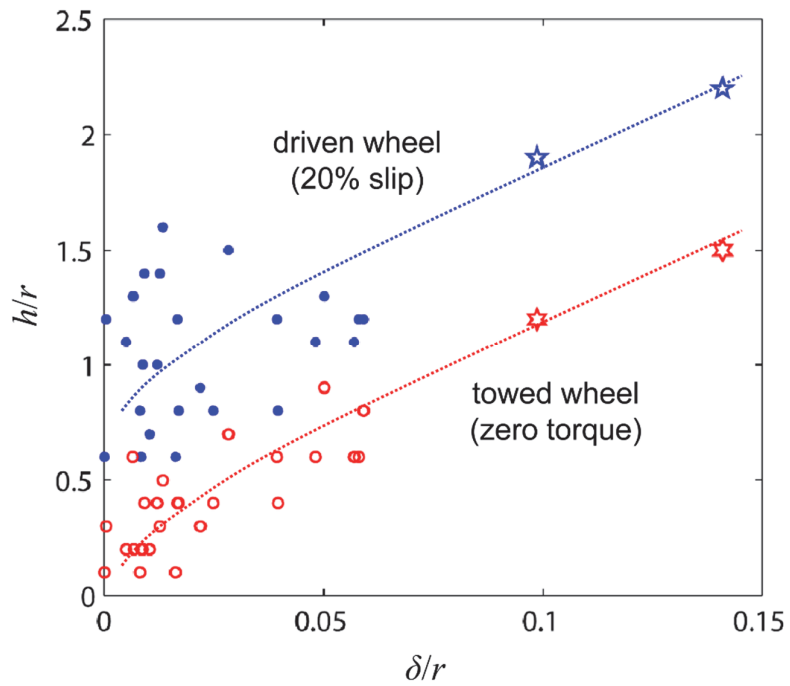


Figure 11. Contact lengths inferred from the test results reported by Freitag (1965) and plotted as a function of wheel penetration (sinkage).

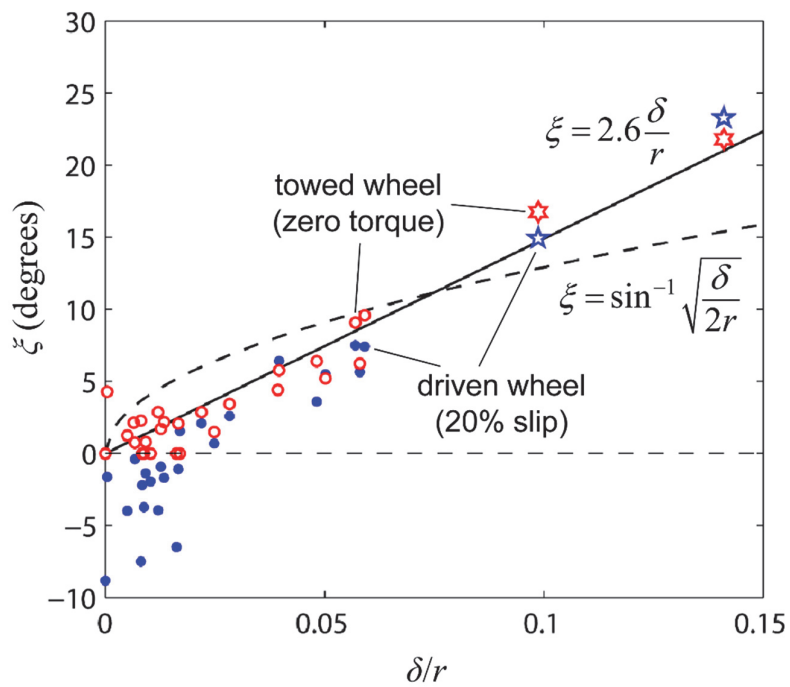


Figure 12. Contact angles inferred from the test results reported by Freitag (1965) and plotted as a function of wheel penetration (sinkage).

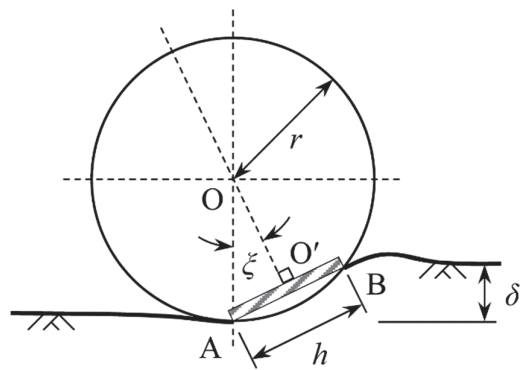


Figure 13. Approximation of contact length h and contact angle ξ as functions of wheel penetration δ (cf. Hambleton and Drescher, 2009a).

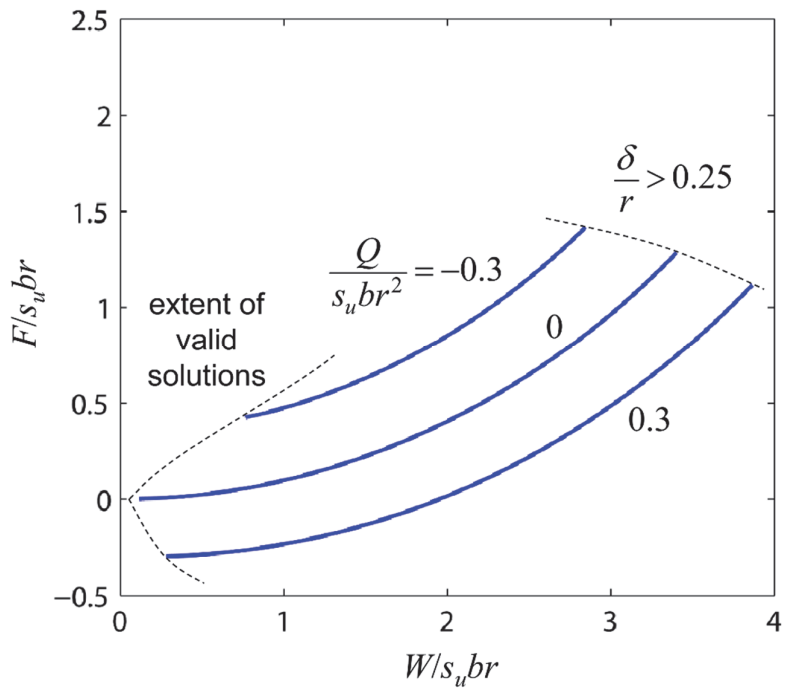


Figure 14. Relationship between horizontal force and vertical force for a braked ($Q < 0$), towed ($Q = 0$), and driven ($Q > 0$) wheel as predicted by the proposed model.

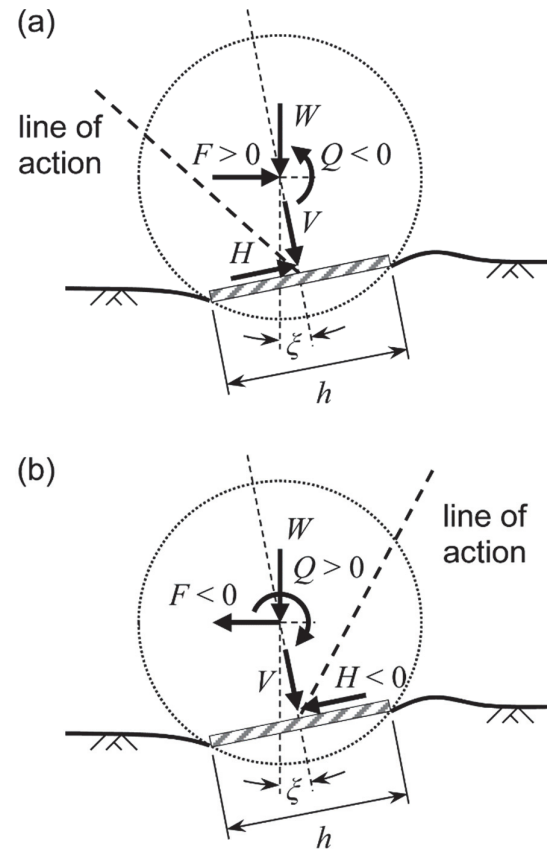


Figure 15. Physical interpretation of the proposed model: (a) braked wheel ($Q < 0$); and (b) driven wheel ($Q > 0$).